ISSUE: June 2010

Comprehensive Flux Estimator Implementation Procedures For Advanced Control Of Inverter-Fed Induction Machines*

by Ali M. Bazzi and Philip T. Krein, Grainger Center for Electric Machinery and Electromechanics, Department of Electrical and Computer Engineering, University of Illinois at Urbana-Champaign, Urbana, Illinois, USA

The trend in motor drives for the last three decades has been to implement vector methods such as field-oriented control (FOC) [1] and direct torque control (DTC) [2]. Advanced control techniques such as feedback linearization [3] are also of interest. Open-loop or V/Hz control is still found in several applications such as small pumps and fans, but drives that require higher performance standards tend to use advanced control methods where energy-saving and optimization methods can also be applied [4, 5]. Several commercial motor drives incorporate vector-based controls to satisfy the growing market demand for higher performance and more-efficient drives.

Most available control techniques for induction machines require information about the flux. For example, FOC requires stator- or rotor-flux estimation in the synchronous frame, DTC requires stator-flux estimation in the stationary frame, feedback linearization requires rotor-flux estimation in the synchronous frame, etc. A typical induction motor drive is shown in Figure 1.

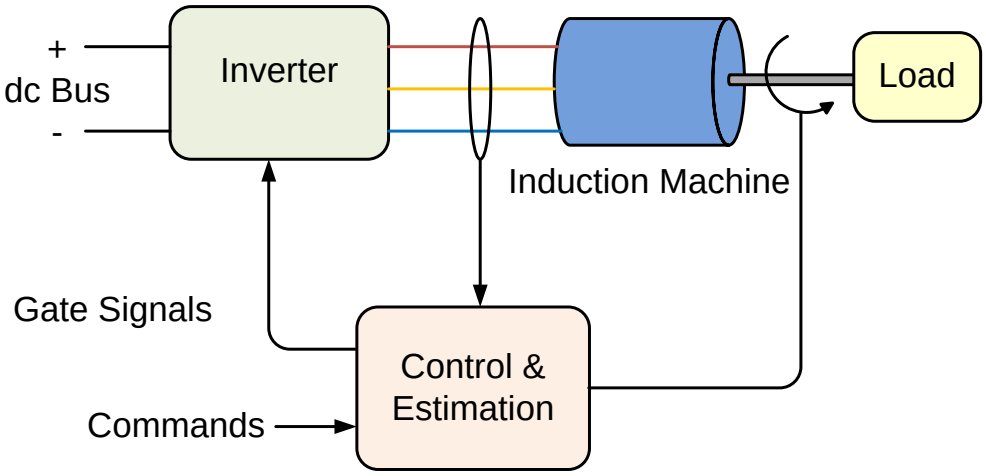

Fig.1. Typical induction motor drive.

The work presented here looks at the estimator as a “gray box” within the Control & Estimation block of Fig. 1. The details of the estimation process are not the purpose of this study, rather general estimator characteristics such as inputs, outputs, estimation error, calibration, and implementation are thoroughly discussed. The back-electromotive force (EMF) estimator was chosen because it is basic and relatively easy to follow for analysis and implementation.

Figure 2 shows a flowchart summarizing the estimator implementation procedure. A similar procedure was used to implement V/Hz and FOC controllers, and this procedure can be extended to other motor control or power electronics applications with a similar digital-control platform. The main steps of the procedure are the preparation of hardware and software, interfacing, implementation, calibration, and testing.

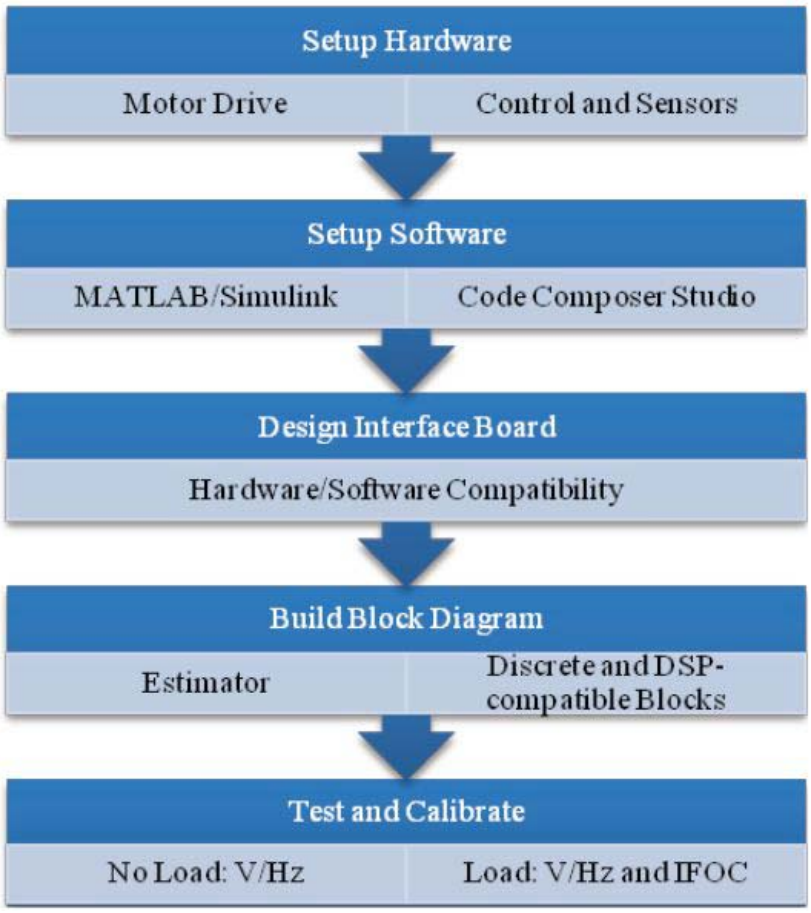

Figure 2. Implementation procedure of the flux estimator.

Flux Estimators

Flux estimators can be categorized into three groups according to [6]: back-EMF methods [6-13], model-reference adaptive systems (MRAS) [14, 15], and observer-based approaches [16-23]. These estimators can have several variations under each category. The list of categories can be extended to include artificial neural networks [24]. Most of the available literature focuses on the ability of estimators to reduce errors in the magnitude and phase of the estimated flux relative to the real flux.

Back EMF estimators are usually based on

$$\lambda^{s}_{qd,s} = \int (v^{s}_{qd,s} - R_s i^{s}_{qd,s})dt. \qquad (1)$$

In (1), $\lambda^{s}_{qd,s}$ is the stator flux linkage in the direct axis, $v^{s}_{qd,s}$ and $i^{s}_{qd,s}$ are the associated voltage and current, and R_S is the stator resistance. These variables are referenced to the stator in the stationary frame, in which voltages and currents can be measured directly. Eq. (1) might result in a dc offset owing to small errors in the voltage and current measurements [11]. The integrator would accumulate these errors and might saturate analog devices or cause an overflow in digital registers. One of the suggested solutions is to use a low-pass filter (LPF) instead of an integrator. However, an LPF will cause both magnitude and phase errors that need compensation [11].

Estimators based on Kalman filters linearize the machine model or restructure the model into a state-space form. Nonlinear observers are more complex and can be designed to produce better estimates [25]. Both sliding-mode observers [21, 23], and Luenberger observers [16, 17, 20] have been presented for flux

estimation applications. Further background on observer-based flux estimators is available in [26].

While most of the available estimators target the stator flux, rotor-flux estimates are also essential in indirect FOC (IFOC). Thus, several rotor-flux estimators have been proposed. A straightforward estimator based on (1) is

$$\lambda^s_{qd,r} = \frac{L_r}{L_m}(\lambda^s_{qd,s} - \sigma L_s i^s_{qd,s})dt. \quad (2)$$

Where $\lambda^s_{qd,r}$ is the rotor-flux linkage, L_m is the magnetizing inductance, L_r is the rotor inductance, and σ is a leakage factor defined as $\sigma = 1 - L_m^2 / L_r L_s$. The estimate from (2) suffers from the same drawbacks as the back-EMF estimator since it is a linear function of $\lambda^s_{qd,s}$. A popular estimator with corrective abilities is presented in [27]. This estimator is given by

$$G = (I - K\frac{L_m}{L_r})\lambda^s_{qd,r} - K\sigma L_s i^s_{qd,s}. \quad (3)$$

$$\lambda^s_{qd,r} = (I - K\frac{L_m}{L_r})^{-1}(G + K\sigma L_s i^s_{qd,s}) \quad (4)$$

where *G* is an intermediate iteration variable, *I* is a 2 x 2 identity matrix, and *K* is a 2 x 2 diagonal estimator gain. The literature does not include a detailed procedure for implementing and calibrating a flux estimator. For example, a digital implementation was employed in [11], but the complete strategy is missing there and the work is difficult to reproduce.

The procedure presented here targets a back-EMF estimator and is divided into three main sections. The first section includes details about the hardware and software requirements. The next section explains the method of implementing and debugging the estimator. And finally, the last section presents calibration, testing, and results.

Software and Hardware Requirements

The work presented here employs a conventional digital-control platform. It is based on the eZdsp F2812 board as a suitable platform for implementing motor controllers. This board is built around the TMS320F2812 digital signal processor (DSP). This platform is compatible with Simulink, and includes six dual pulse-width-modulation (PWM) channels (12 channels total), 16 analog-to-digital converters (ADCs), and a speed-encoder input [28]. The processor is a 32-bit DSP with fixed-point arithmetic; thus, discrete and fixed-point math blocks from Simulink can be used to program it.

Software Requirements

Two primary software packages must be available on the host computer where the development and control take place: MATLAB/Simulink, which support math and control development, and Code Composer Studio (CCS), which supports detailed code development for the DSP. Compatibility is essential. For example, MATLAB 7.0.4 must be used with CCS 2.21, MATLAB 2006a must be used with CCS 3.1, etc. Simulink provides a simple user interface where a designer can build the estimator using discrete-time blocks and special DSP-related blocks from the "C2000" library, such as the fixed-point math "C28x IQmath" library.

Simulink is able to compile a block diagram into C code and then call CCS to generate assembly code for the DSP. A project is generated in CCS to be loaded into the DSP. MATLAB can also be used to build a friendly guided user interface (GUI) for real-time communication with the DSP through its parallel port using real-time

data exchange channels (RTDX). These channels are set in the block diagram to be assigned in the DSP. Figure 3 shows a summary of the setup. It is important to note that programmers with experience in C or assembly languages can write their own optimized code for the DSP with basic tools, but this is a time-consuming process.

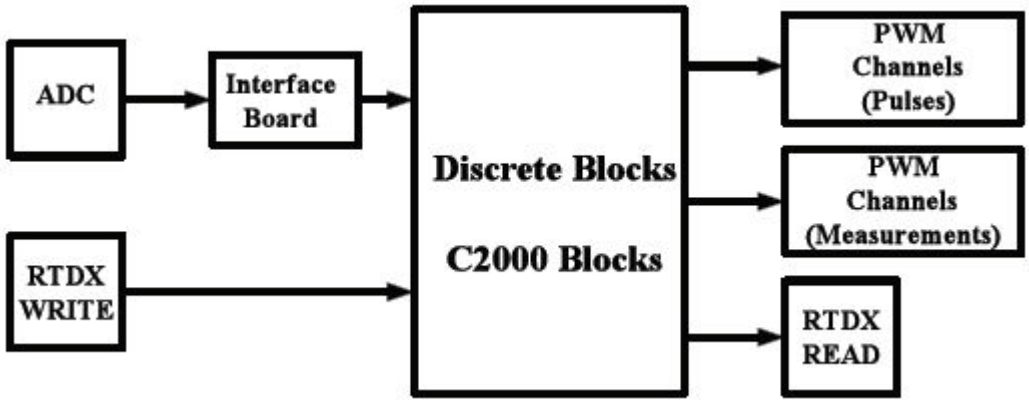

Figure 3. Hardware and software interconnections.

Hardware Requirements

The only special hardware requirements for flux estimation are the host computer and the DSP board. The eZdsp used here is also able to operate offline from the computer, since it operates from an independent power supply. Current and voltage sensors are built into the power stage of the inverter in most advanced motor drives. The procedure presented here can be easily modified to other DSPs used as motor-control platforms.

The sensors required by the estimator vary depending on the application and the estimation process. For example, DTC requires the stator-flux estimate in the stationary frame; thus stator voltages and currents are necessary. For IFOC, voltage sensors might not be required, but a speed encoder is needed. Each advanced control technique has a minimum sensor requirement. The requirements are not likely to exceed three voltage sensors, four current sensors with one measuring the neutral current, and a speed encoder.

The interface board shown in Figure 3 may be needed, depending on the compatibility of the sensors with the DSP, and could be placed before and/or after the ADC depending on the ADC's electrical characteristics. When inserted before the ADC, this board takes the sensor outputs and conditions them for the ADC. For example, the ADC on the eZdsp F2812 requires all inputs to the ADC to be between 0 and 3 V [28]. While simple voltage dividers with limited currents are straightforward, many current sensors have dc offsets and special input/output relations.

Figure 4 shows a sample current-sensor characteristic and the expected output of the interface board fed into the eZdsp. If an external ADC is used, its output might need to be interfaced with the DSP through another interface board shown in Fig. 3. The scaling circuitry usually consists of simple op-amp adders, gains, and filters. Additional digital filters on the DSP may be used to eliminate small offsets.

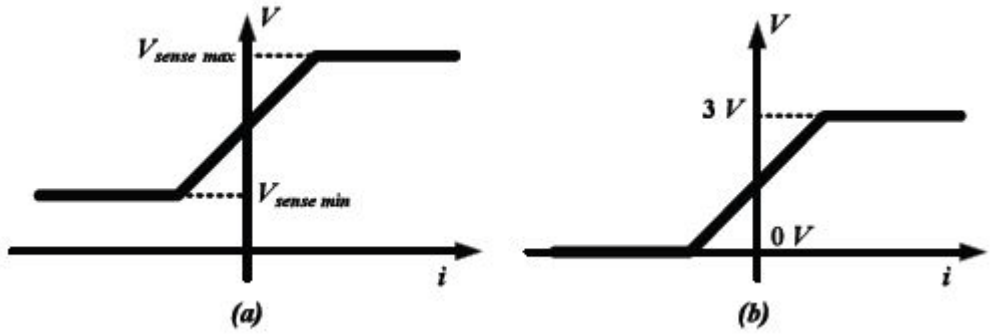

Figure 4. Sensor output (a) and scaled sensor output compatible with the DSP (b).

Implementation Procedure

After the sensors are scaled and conditioned for the ADC, the designer can read hardware information into Simulink. The outputs from Simulink are usually the PWM channels on the DSP—six dual channels, three of which are used to control the three-phase inverter, leaving three for measurements. The PWM outputs are discrete-valued, but the underlying modulation signal can be extracted with appropriate filtering. Other measurements can be made using the RTDX where the signals are sent from the DSP to the computer. RTDX can either read or write; thus, with an appropriate GUI, the designer can measure and send commands to the DSP in real time. The target eZdsp, and sample ADC, PWM, and RTDX blocks from Simulink are shown in Figure 5.

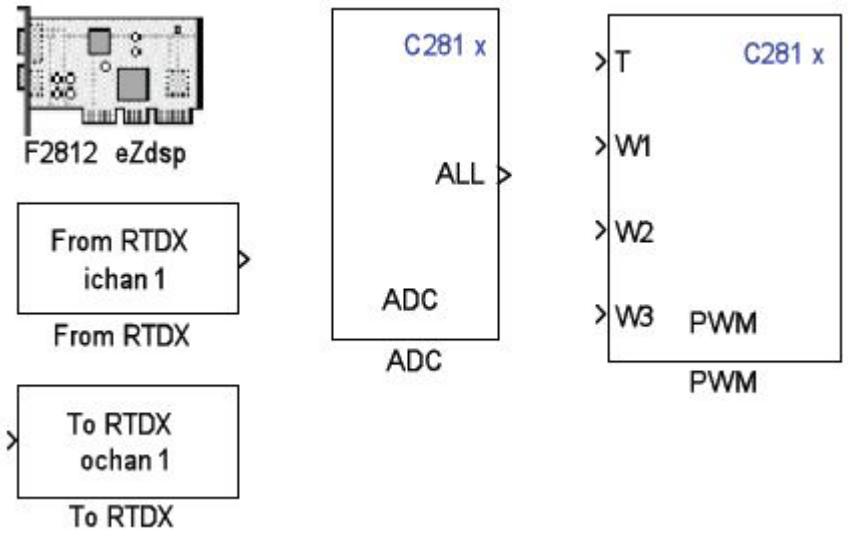

Figure 5. Sample DSP-related blocks in Simulink.

When the hardware and MATLAB/Simulink and CCS are installed, building the estimator can start. The target hardware needs to be selected from the "C2000 Target Preferences" library. An important step is to set a discrete step size for the simulator. In general, smaller step sizes are better, provided the computational burden can be managed. In this system, the DSP clock frequency is 150 MHz. In the flux-estimator application, a sampling time of T_S =30 µs is feasible with this clock rate.

The ADC has two modules, A and B, which can be accessed using the "ADC" block found in the "C28x DSP Chip Support" library. The sampling rate of the ADC can go up to 12.5 MHz, depending on the number of channels being read. The flux estimator here uses seven channels; thus a low sampling rate should be used [29]. It is important to mention that the encoder input is separate from the ADC on this DSP.

The ADC output is an array that must be demultiplexed to recover the individual signals. Its data type is an unsigned 16-bit integer. Only twelve bits are used by the ADC, however, where an analog level of 3 V corresponds to 4096, the full-scale 12-bit representation. This poses the need for appropriate software scaling. An example is shown in Figure 6.

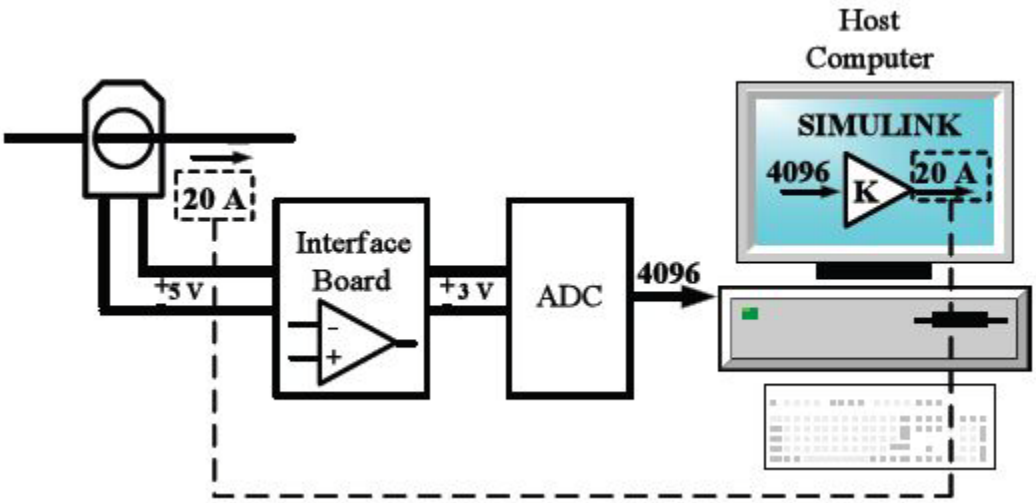

Figure 6. An example of a scaling procedure for a sensor output.

A current of 20 A translates to 5 V, before scaling to 3 V for DSP compatibility. The internal scale factor must be 20/4096 to translate the ADC output into current at 20 A full scale. To achieve the best decimal accuracy, fixed-point math is used on the DSP. The "Target for TI C2000" Simulink library has the "C28x IQmath" module in which basic accurate math operations can be found [30].

The *Q* value of an IQ number is the bit before which the decimal point is placed. IQMATH blocks accept signed 32-bit fixed-point integers (sfix(32)). Figure 7 shows a sample of an sfix(32) number with *Q* =29. All data types must be converted to sfix(32) numbers to be implemented in the DSP. A detailed description of the IQMATH library is available in [30].

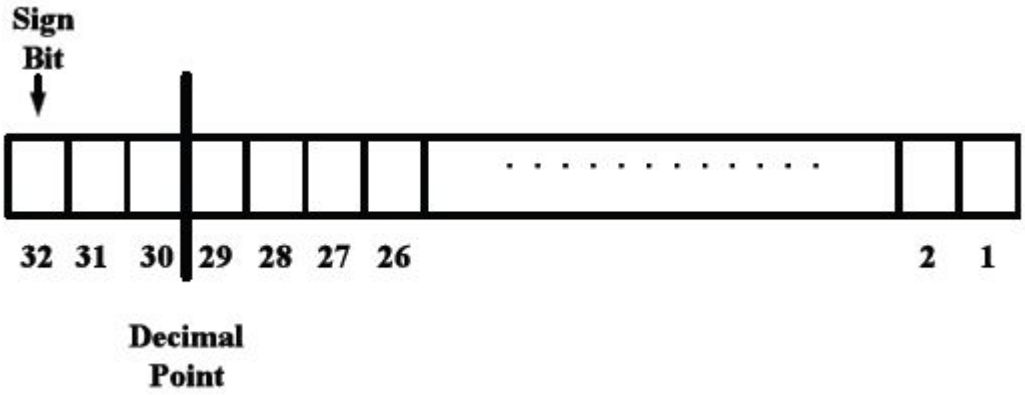

Figure 7. 32-bit signed fixed-point number.

The implementation of (1) is straightforward except for the integrator. Several back-EMF estimators replace it with an LPF because of the integrator dc offset. We used a discrete-time integrator sampled at T_S, and as expected, the dc offset existed and caused the integrator output to grow without bound. To solve this problem, the scheme shown in Figure 8 was implemented, where z is a one-unit delay. An LPF is added to extract the dc offset, which is first reduced by the high-pass filter (HPF).

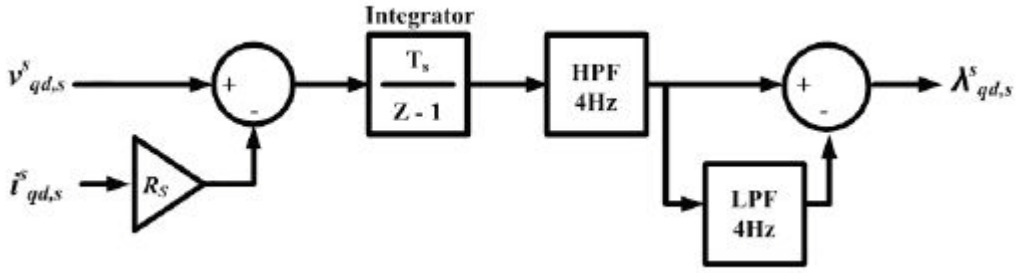

Figure 8. Modified flux estimator.

The rotor flux is estimated using (2). All constants need to have the sfix(32) data type for accurate values. For example, the leakage term, σ, has a value close to 1, so Q = 30 is used to represent it. On the other hand, the stator voltages have significantly higher values and can be represented with a smaller Q. The rotor flux in the synchronous frame is found by using Park's transformation [1]. The cosine and sine terms need to have Q = 30 for highest precision since their values are between -1 and 1. An example of an IQmath application is the rotor angle ρ found using the "Arctangent IQN" block, based on

$$\rho = \tan^{-1}\left(\frac{\lambda^s_{q,r}}{\lambda^s_{d,r}}\right) \qquad (5)$$

To further improve the estimation and achieve a higher accuracy, the flux is estimated in mVs. This gives more room for decimal bits in the 32-bit number.

Testing And Results

The flux estimator described in (1) and (2) was implemented with a scheme similar to the one shown in Figure 8. All the blocks utilized in Simulink were as described in the previous sections, and the hardware setup is shown in Figure 9. The eZdsp board and the interface board are shown in Figure 10.

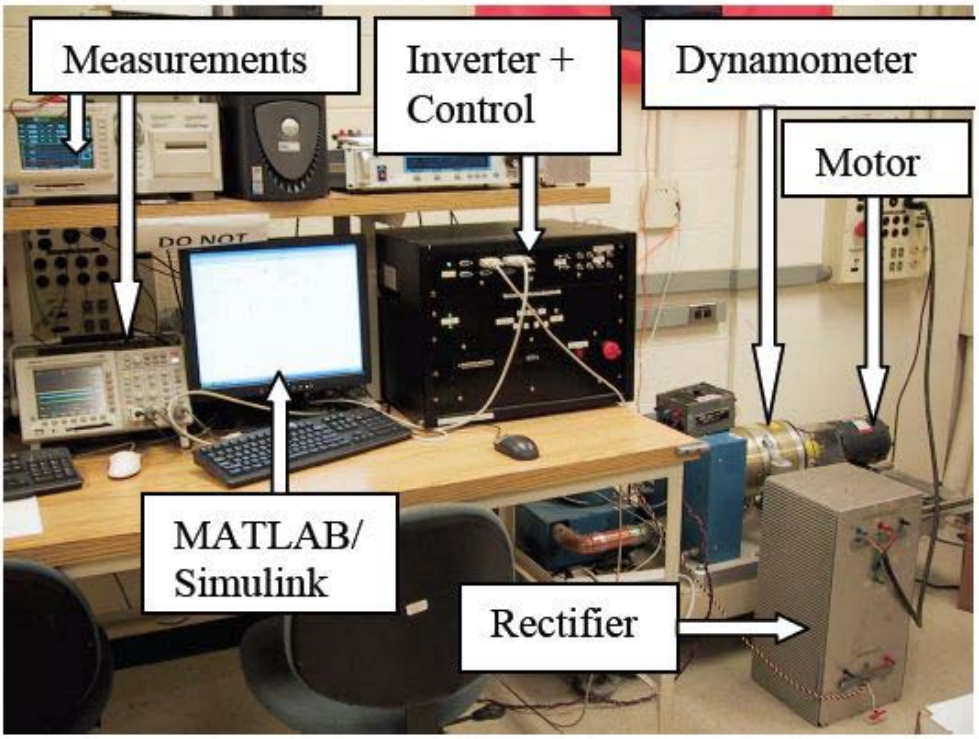

Figure 9. Hardware setup.

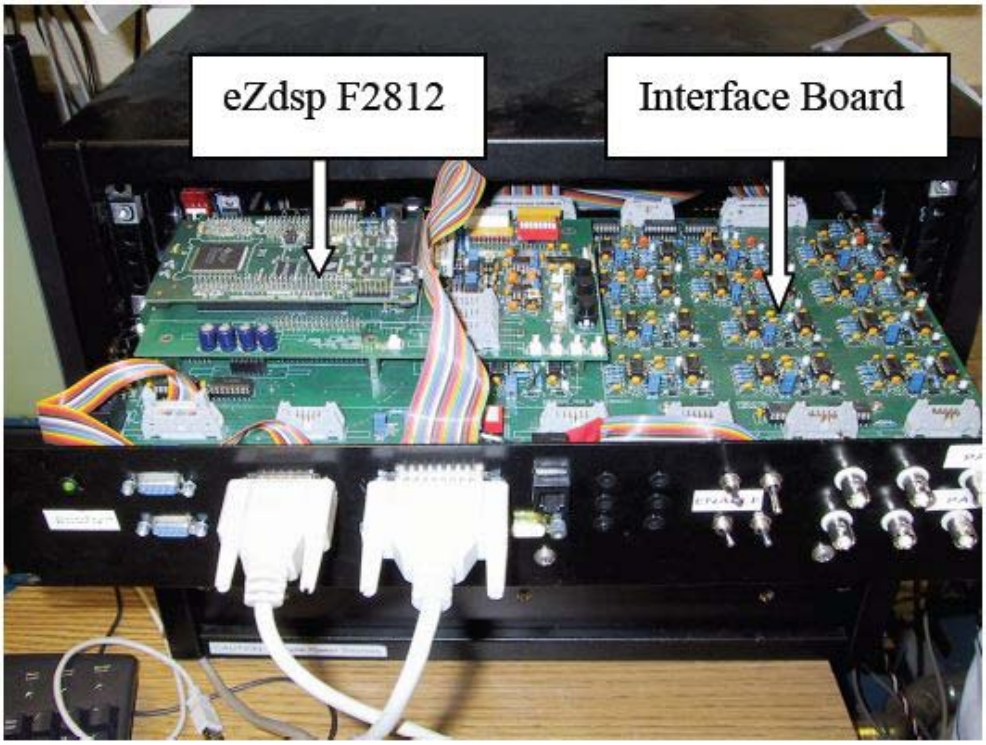

Figure 10. eZdsp board and the interface board.

The fluxes computed by the estimator were fed into RTDX channels to be plotted and saved in real time. The results need to be checked for accuracy against a reference flux. The first procedure simulates the motor drive and estimator in Simulink, with the same step size as the sampling rate of the hardware. Significant errors existed between the hardware and simulation. The main issues are:

1) Use of an ideal simulation model.

2) Quantization errors.

The simulation model used was ideal in several ways. No saturation or core-loss models were added, which affected the flux-current relationships. The inverter was simulated as an ideal amplifier, and the lines interconnecting the system were lossless. Also, noise effects, which might be significant, were ignored. Quantization errors can cause significant problems, especially with the integrator. An example is shown in Figure 11 where part of a sine wave is drawn. To reduce the quantization error, a higher ADC sampling rate can be used, without violating the sampling limit [29].

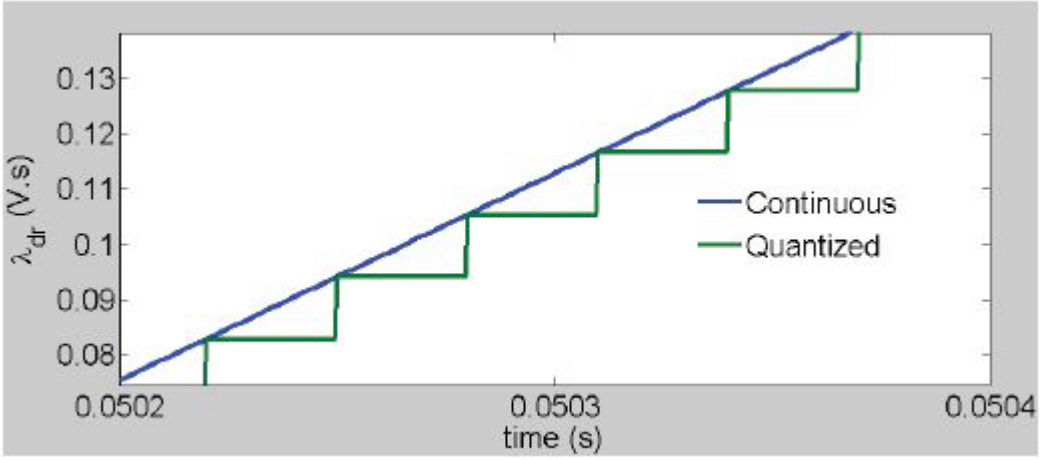

Figure 11. Quantized versus continuous flux.

To account for the non-ideal real-life situation, another simulation approach was used. The rms terminal voltages and line currents of the motor were measured from experiments. The measured values in effect take into account all losses and nonlinearities. These results were then fed into a simulation implementing (1) and (2) at a high sampling rate, resembling continuous time relative to T_S. The results from this simulation give a clear idea about the quantization errors in the system. The sampling time was 25 µs for V/Hz and 30 µs for IFOC in simulations and experiments. The switching frequency for the V/Hz was 10 kHz; IFOC used hysteretic control.

The main comparison between the simulations and experiments was made under V/Hz with no load. The other tests were made with a load under V/Hz and IFOC.

V/Hz With No Load

The stator current is low, and the effect of the stator voltage drop is negligible. This reflects a relatively ideal V/Hz control with low losses. This test has a predictable peak stator flux; thus experimental and simulation results can be compared to theory if needed. Table 1 summarizes the peaks of the stator and rotor fluxes in simulations (Sim.) and experiments (Exp.), for low and high speeds. Figures 12 and 13 show the simulation and hardware results. The errors in Table 1 are very low and reflect an acceptable estimation. The error could be a result of quantization errors and inaccuracies in motor parameters.

Table 1. Flux peaks from simulations and experiments under V/Hz with no load.

	1226 rpm (42 Hz)			600 rpm (20.7 Hz)		
	Sim.	Exp.	Error	Sim.	Exp.	Error
$\lambda_{d,s}^{s}$	415	400	3.6%	325	350	7.7%
$\lambda_{d,r}^{s}$	410	390	4.9%	320	310	3.2%

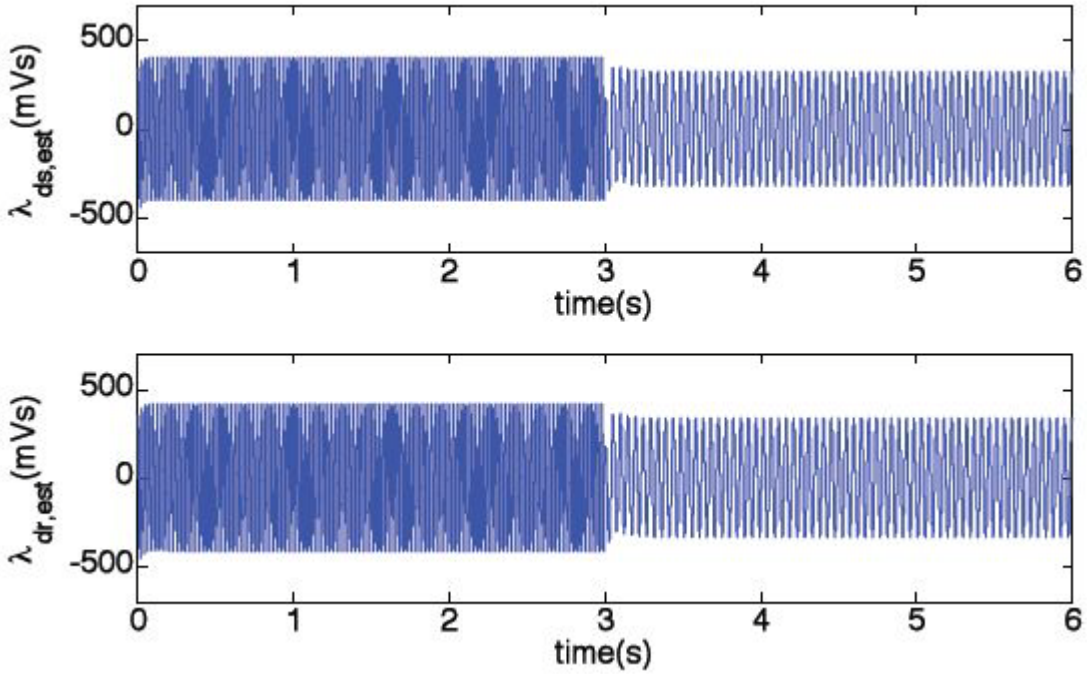

Figure 12. Simulation results for d-axis stator and rotor fluxes under V/Hz with no load.

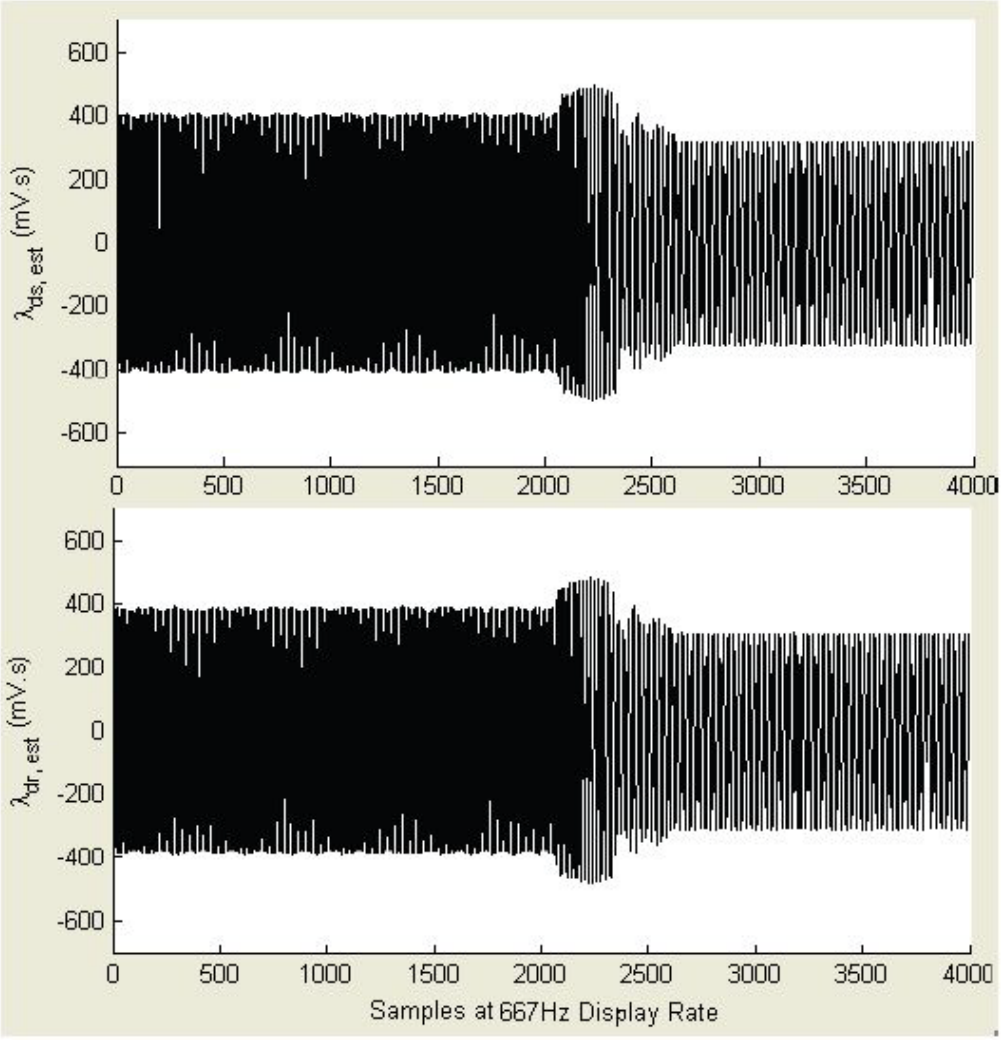

Figure 13. Hardware results for d-axis stator and rotor fluxes under V/Hz with no load.

It is time consuming to synchronize the hardware and simulations to consider the phase shift, φ. Thus, a simple approach is to predict the phase shift due to the first-order high-pass filter (HPF) at 4 Hz with transfer function $H(j\omega)$ where ω is the frequency in rad/s. For example, if the flux is at 60 Hz, the phase shift, φ, can be predicted as

$$H(j\omega) = \frac{j\omega}{j\omega + 2\pi 4} \tag{6}$$

$$\varphi = \tan^{-1}(2\pi 60) - \tan^{-1}\left(\frac{2\pi 60}{2\pi 4}\right) = 89.58° \tag{7}$$

The phase shift due to the LPF is negligible with about 1.54°. Thus the effect of the HPF can be easily predicted and compensated for by about 90°.

V/Hz with Load

To account for the effects of loads and higher losses that result under loading conditions on the flux estimator, the motor was loaded under different speeds. At a speed of 1226 rpm, the load torque was 3 Nm, while at 600 rpm, the load torque was 0.7 Nm. A similar procedure to the no-load case was followed, and the results are

shown in Table 2 and Figures 14 and 15. Figure 16 shows the experimental torque and speed plots. The results show that the flux-estimation error under load is higher but is still around 10%. The main issue is believed to be parameter error especially because the rotor time constant and the stator resistance vary under load where the motor temperature increases.

Table 2. Flux peaks from simulations and experiments under V/Hz with load.

	1226 rpm (42 Hz), 3 Nm			600 rpm (20.7 Hz), 0.7 Nm		
	Sim.	Exp.	Error	Sim.	Exp.	Error
$\lambda^s_{d,s}$	355	315	11.3%	301	290	3.7%
$\lambda^s_{d,r}$	345	305	11.6%	295	265	10.2%

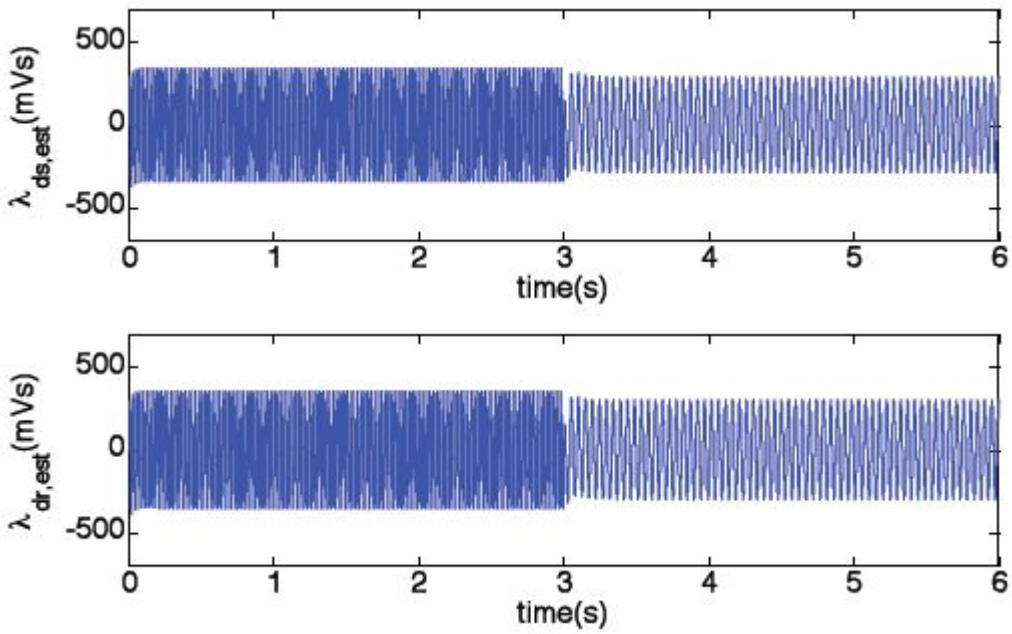

Figure 14. Simulation results for d-axis stator and rotor fluxes under V/Hz with load.

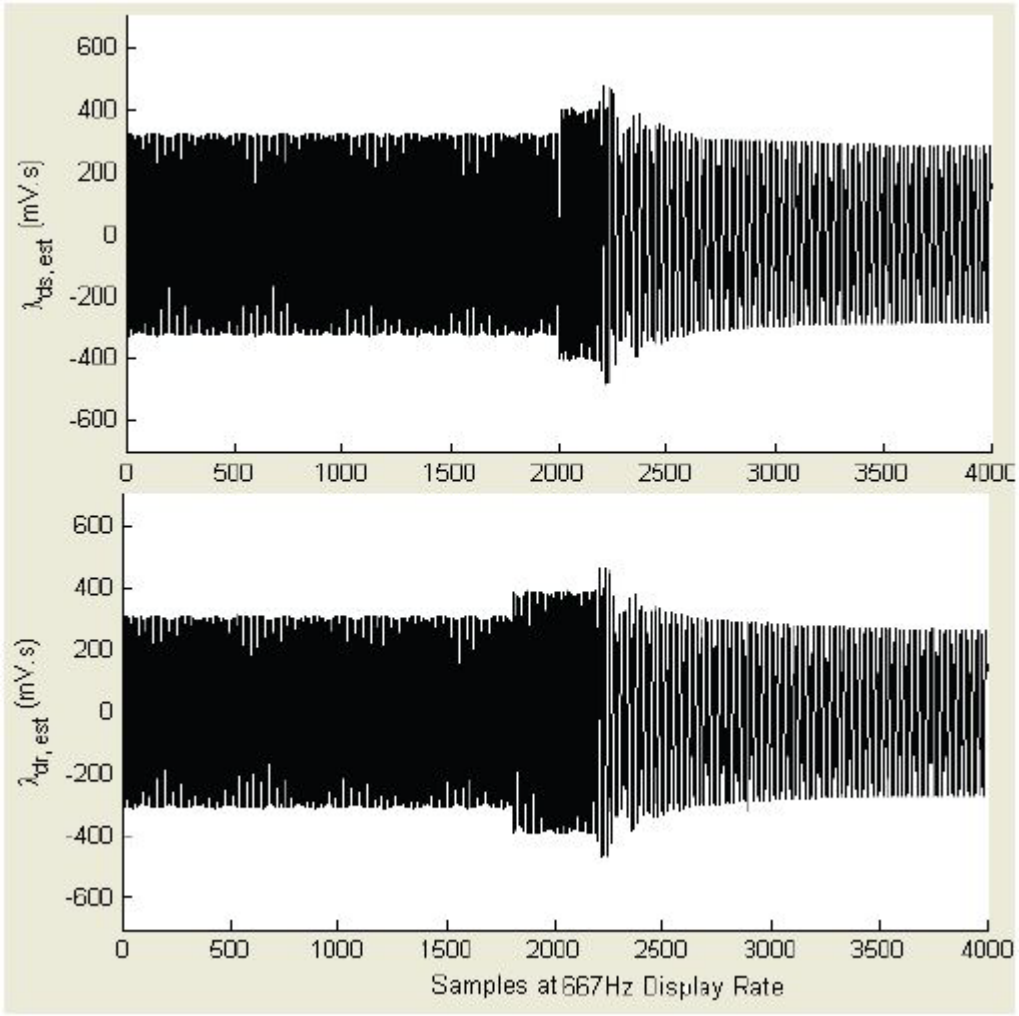

Figure 15. Hardware results for d-axis stator and rotor fluxes under V/Hz with load.

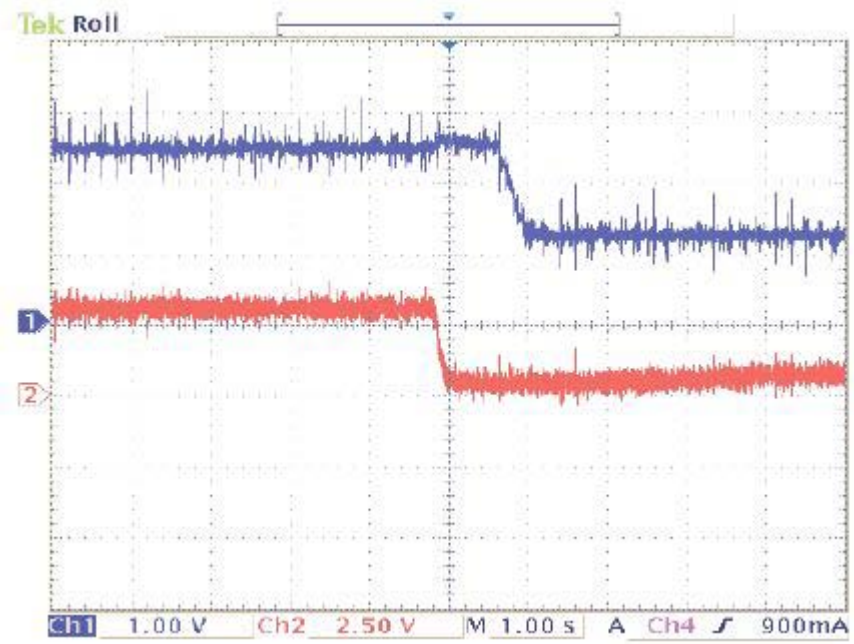

Figure 16. Speed (Ch1: 500 rpm/div) and torque (Ch2: 2 Nm/div) under V/Hz.

IFOC With Load

The last test with IFOC requires a flux estimate. The command flux is 500 mVs. This test needs special calibration due to the noise and uncontrolled switching under hysteresis. The currents and voltages under IFOC have higher harmonic content than fixed PWM in V/Hz control; therefore, quantization errors are more significant. Running the estimator in simulation and hardware without any calibration resulted in estimation errors of more than 30%. To compensate for quantization errors and noise, simple calibration was needed. A constant gain of 8/7 was used in the stator estimator to achieve better flux estimates. The value of the gain was determined by running the simulations and hardware, then comparing the peaks and scaling the stator flux.

Table 3 shows the errors in the peaks from experiments and simulations, and Figures 17 and 18 show the actual and estimated fluxes. Figure 19 shows the experimental torque and speed plots. The results in Table 3 have a low error rate even though the estimation is performed under hysteretic control. The calibration of the gain is straightforward and can be further improved. For example, a look-up table of gains can be used for different operating conditions.

Table 3. Flux peaks from simulations and experiments under IFOC with load.

	1226 rpm (42 Hz), 3 Nm			600 rpm (20.7 Hz), 0.7 Nm		
	Sim.	Exp.	Error	Sim.	Exp.	Error
$\lambda^s_{d,s}$	394	400	1.5%	460	430	7%
$\lambda^s_{d,r}$	384	385	0.26%	448	415	8%

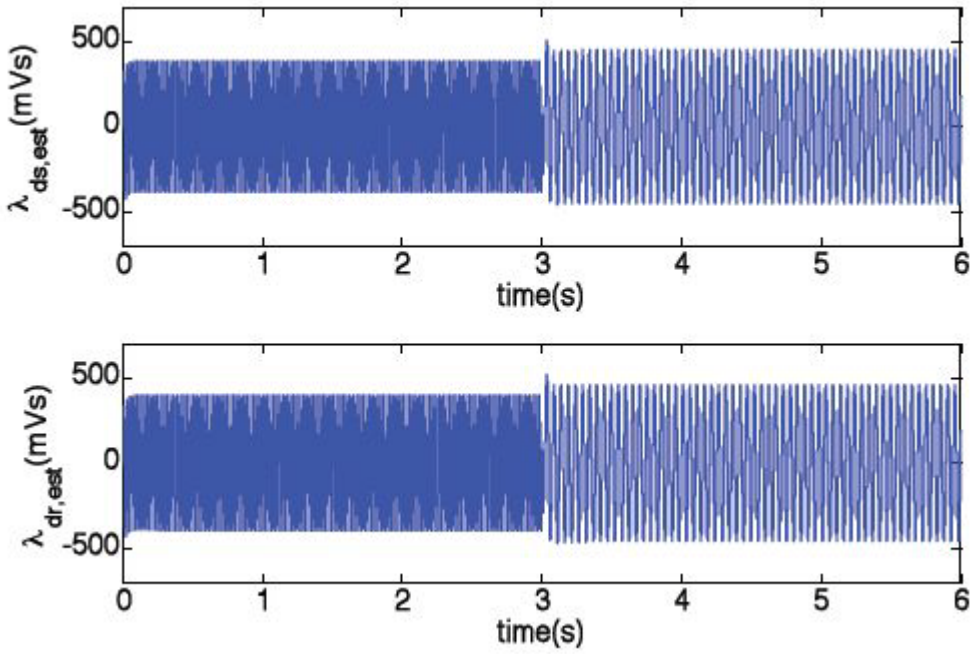

Figure 17. Simulation results for d-axis stator and rotor fluxes under IFOC with load.

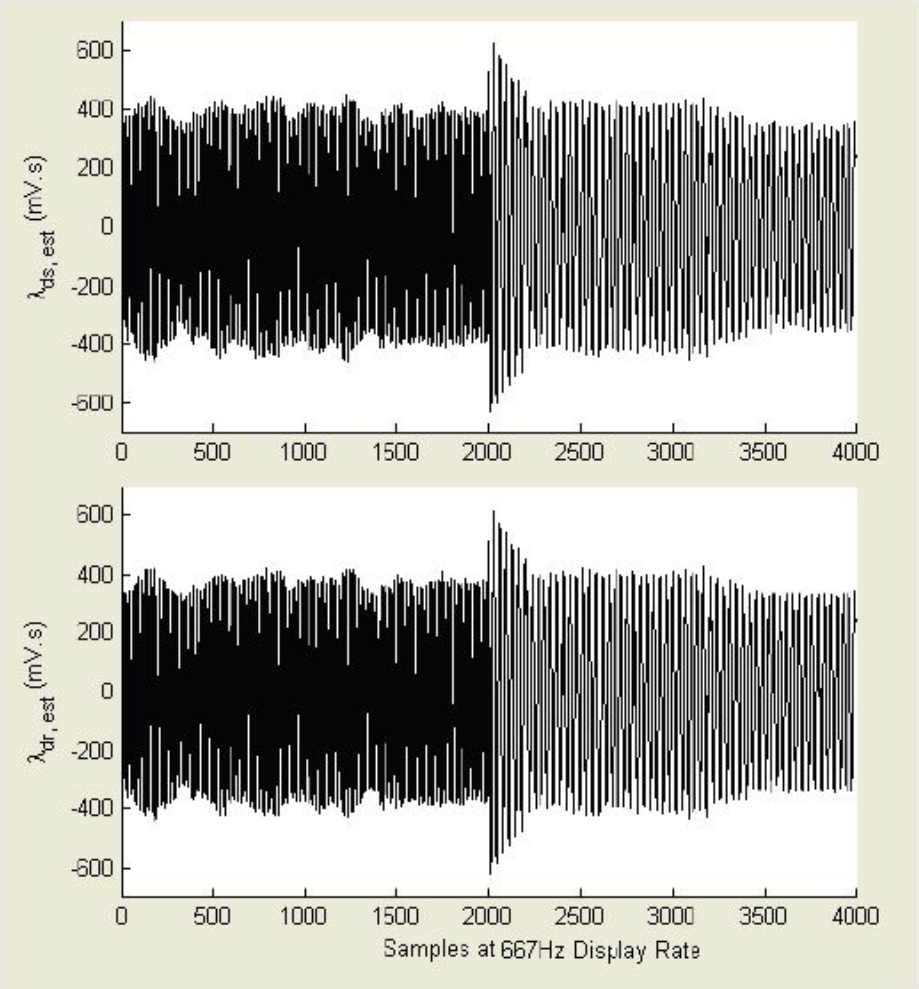

Figure 18. Hardware results for d-axis stator and rotor fluxes under IFOC with load.

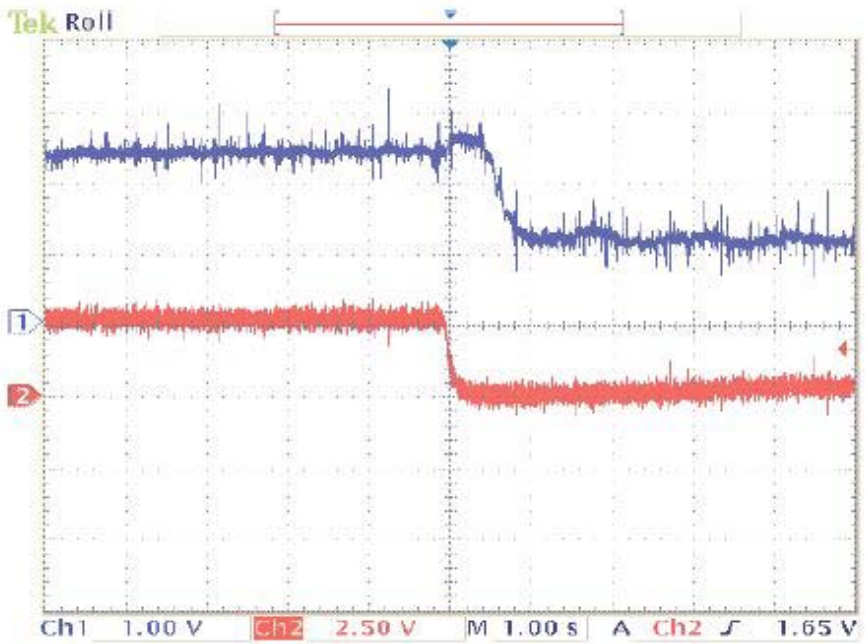

Figure 19. Speed (Ch1: 500 rpm/div, upper trace) and torque (Ch2: 2 Nm/div, lower trace) under IFOC.

Conclusion

A comprehensive procedure for the implementation of a flux estimator was presented. The procedure is based on using a DSP as a control and estimation platform for inverter-fed induction machines. Hardware and software requirements, interfacing procedures, implementation, calibration, and testing were all presented. Detailed but simplified discussions of the fixed-point processing requirements for motor drives and other power electronics applications were also presented. This procedure can be used for several other applications where real-time DSP control and estimation are required.

Acknowledgement

This work is supported in part by the Granger Center for Electric Machinery and Electromechanics at the University of Illinois, and by the Office of Naval Research under grant ONR N00014-08-1-0397. The authors would like to acknowledge the valuable help of Mr. Kevin Colravy and Mr. Sanghun Choi.

**This paper was originally presented at the 2009 Electrical Manufacturing & Coil Winding Expo, held September 29-October 1, 2009 in Nashville, Tenn. For more information, see http://www.emcwa.org/.*

References

1. P. C. Krause, O. Wasynczuk, and S. D. Sudhoff, Analysis of Electric Machinery and Drive Systems, 2nd ed. New York: Wiley - IEEE Press, 2002.
2. I. Takahashi and Y. Ohmori, "High-performance direct torque control of an induction motor," IEEE Trans. Industry Applications, vol. 25, pp. 257 - 274, Mar. 1989.
3. P. T. Krein, F. Disilvestro, I. Kanellakopoulos, and J. Locker, "Comparative analysis of scalar and vector control methods for induction motors," in Rec, IEEE Power Electronics Specialists Conf., 1993, pp. 1139 - 1145.
4. A. M. Bazzi and P. T. Krein, "Input power minimization of an induction motor operating from an electronic drive under ripple correlation control," in Proc. IEEE Power Electronics Specialists Conf., 2008, pp. 4675 - 4681.
5. D. S. Kirschen, D. W. Novotny, and T. A. Lipo, "On-Line Efficiency Optimization of a Variable Frequency Induction Motor Drive," IEEE Trans. Industry Applications, vol. IA-21, pp. 610 - 616, May 1985.
6. A. B. Nikolic and B. I. Jeftenic, "Fixed-point DSP algorithm for flux estimation in DTC IM drive," in Proc. International Conference on Computer as a Tool, 2005, pp. 1582 - 1585.
7. D. A. Andrade, A. W. F. V. Silveira, P. B. Severino, and T. S. Tavares, "Dsp based torque estimation in three-phase cage induction motors," in Proc. IEEE International Electric Machines and Drives Conference, 2007, pp. 1726 - 1731.
8. A. Consoli, G. Scarcella, and A. Testa, "Speed - and current-sensorless field - oriented induction motor drive operating at low stator frequencies," IEEE Trans. Industry Applications, vol. 40, pp. 186 - 193, Jan. 2004.
9. O. S. Ebrahim, P. K. Jain, and A. Bakhshai, "Optimal state control of induction machine with improved stator flux estimation," in Proc. IEEE Applied Power Electronics Conference and Exposition, 2009, pp. Feb. 15 - 19.
10. A. Gastli, M. Tomita, T. Takeshita, and N. Matsui, "Improvement of a stator-flux-oriented speed sensorless control of an induction motor," in Proc. Power Conversion Conference, 1993, pp. 415 - 420.
11. M. Kaliamoorthy, S. Himavathi, and A. Muthuramalingam, "DSP based implementation of high performance flux estimator for speed sensorless induction motor drives using TMS320F2812," in Proc. India International Conference on Power Electronics, 2006, pp. 104 - 109.
12. Y. Li, W. Huang, and Y. Hu, "A low cost implementation of stator-flux-oriented induction motor drive," in Proc. International Conference on Electrical Machines and Systems, 2005, pp. 1534 - 1538.
13. D. O. Neacsu and K. Rajashekara, "Comparative Analysis of Torque-Controlled IM Drives with Applications in Electric and Hybrid Vehicles," IEEE Trans. Power Electronics, vol. 16, pp. 240 - 247, Mar. 1998.
14. G. J. Armstrong, D. J. Atkinson, and P. P. Acarnley, "A comparison of estimation techniques for sensorless vector controlled induction motor drives," in Proc. International Conference on Power Electronics and Drive Systems, 1997, pp. 110 - 116.
15. M. Elbuluk, N. Langovsky, and M. D. Kankam, "Design and Implementation of a Closed-Loop Observer and Adaptive Controller of Induction Motor Drives," IEEE Trans. Industry Applications, vol. 34, pp. 435 - 443, May 1998.
16. T. Du and M. A. Brdys, "Implementation of extended luenberger observers for joint state and parameter estimation of pwm imduction motor drive," in Proc. European Conference on Power Electronics and Applications (EPE), 1993, pp. 439 - 444.
17. D. G. Forchetti, G. O. Garcia, and M. I. Valla, "Sensorless Control of Stand - Alone Doubly Fed Induction Generator with an Adaptive Observer," in Proc. IEEE International Symposium on Industrial Electronics, 2008, pp. 2444 - 2449.
18. L. Harnefors, "Design and Analysis of General Rotor-Flux-Oriented Vector Control Systems," IEEE Trans. Industrial Electronics, vol. 49, pp. 383 - 390, Apr. 2001.

19. M. Hilairet, F. Auger, and C. Darengosse, "Two efficient kalman filters for flux and velocity estimation of induction motors," in Proc. IEEE Power Electronics Specialists Conference, 2000, pp. 891 - 896.
20. C. Manes, F. Parasiliti, and M. Tursini, "DSP based field oriented control of induction motor with a nonlinear state observer," in Rec. IEEE Power Electronics Specialists Conference, 1996, pp. 1254 - 1259.
21. S. Sangwongwanich, T. Yonemoto, and S. Okuma, "Time domain characteristics of sliding observer for flux estimation of induction motor and its implementation," in Rec., IEEE Power Electronics Specialists Conference, 1991, pp. 591 - 595.
22. H. Weng, C. Liu, F. Li, and L. Wei, "A new flux observer of induction motor by H∞ optimization," in Rec., IEEE Industry Applications Conference, 2001, pp. 1795 - 1799.
23. Z. Yan and V. Utkin, "Sliding mode observers for electric machines - an overview," in Proc. Annual Conference of the IEEE Industrial Electronics Society, 2002, pp. 1842 - 1847.
24. J. O. P. Pinto, B. K. Bose, and L. E. B. Silva, "A statorflux-oriented vector-controlled induction motor drive with space-vector pwm and flux-vector synthesis by neural networks," IEEE Trans. Industry Applications, vol. 37, pp. 1308 - 1318, Oct. 2001.
25. C. Manes, F. Parasiliti, and M. Tursini, "A comparative study of rotor flux estimation in induction motors with a nonlinear observer and the extended kalman filter," in Proc. IEEE International Conference Industrial Electronics, Control and Instrumentation, 1994, pp. 2149 - 2154.
26. L. A. Pereira, J. F. Haffner, E. M. Hemerly, and H. A. Grundling, "A simulation framework for flux estimation and vector control of induction machines," in Proc. Annual Conference of the IEEE Industrial Electronics Society, 1998, pp. 1587 - 1591.
27. G. C. Verghese and S. R. Sanders, "Observers for Flux Estimation in Induction Machines," IEEE Trans. Industrial Electronics, vol. 35, pp. 85 - 94, Feb. 1988.
28. "eZdsp(TM) F2812 Technical Reference 506265-0001 Rev. F," Spectrum Digital, Stafford, TX 2003.
29. A. Tessarolo, "F2810, F2811, and F2812 ADC Calibration," Texas Instruments, Dallas, TX 2004.
30. "C28x IQmath Library: A Virtual Floating Point Engine V1.5a," Texas Instruments Dallas, TX 2009.

About The Authors

Ali M. Bazzi *received the B.E. degree in electrical engineering in June 2006 (with high distinction), and the M.E. degree in electrical engineering in July 2007 from the American University of Beirut, Lebanon. Since August 2007, he has been pursuing the Ph.D. in electrical engineering at the University of Illinois at Urbana-Champaign.His research interests are power electronics applications in motor drives and renewable energy, mainly in the fields of control and optimization. He was the conference director of the 2010 Power and Energy Conference at Illinois, and is currently the chair of the IEEE PELS/PES joint Student Chapter at the University of Illinois at Urbana-Champaign. He is a student member of the IEEE, and a member of the IEEE Power Electronics Society, and IEEE Industry Applications Society, and IEEE Power and Energy Society.*

Philip T. Krein *received the B.S. degree in electrical engineering and the A.B. degree in economics and business from Lafayette College, Easton, Pennsylvania, and the M.S. and Ph.D. degrees in electrical engineering from the University of Illinois, Urbana. He was an engineer with Tektronix in Beaverton, Oregon, then returned to the University of Illinois. At present he holds the Grainger Endowed Director's Chair in Electric Machinery and Electromechanics as director of the Grainger Center for Electric Machinery and Electromechanics. His research interests address all aspects of power electronics, machines, and drives, with emphasis on nonlinear control approaches. He published an undergraduate textbook, Elements of Power Electronics (Oxford University Press, 1998). In 2001, he helped initiate the International Future Energy Challenge, a major student competition involving fuel cell power conversion and energy efficiency for machines. He holds twelve U.S. and four European patents. Dr. Krein is a registered professional engineer in Illinois and in Oregon. He was a senior Fulbright Scholar at the University of Surrey in the United Kingdom in 1997-98, and was*

recognized as a University Scholar in 1999, the highest research award at the University of Illinois. In 2003 he received the IEEE William E. Newell Award in Power Electronics. From 2005 to 2007 he was a Distinguished Lecturer of the IEEE Power Electronics Society.